Supporting information

Long-Cycle Stable Operation of Fluoride-Ion Batteries at Room Temperature Enabled by Advanced Interface Engineering and Ion Diffusion Kinetics Regulate Strategy

Jia Xiang[†,a], *Meiyan Chen* [†,c], *Ying Lei*[†,b], *Jun Zhou*[4],*d Wei Zou*[*,b], *Rongwen Lu*[*,a], *Shufen Zhang* [a]

[a] State Key Laboratory of Fine Chemicals, Frontiers Science Center for Smart Materials, School of Chemical Engineering, Dalian University of Technology, Dalian 116024, P.R. China

[b] College of Chemistry and Engineering, Sichuan University of Science and Engineering, Zigong 643000, P R China.

[c] Southwestern Institute of Physics, Chengdu 610225, P. R. China.

[d] Engineering Center of Integrated Optoelectronic & Radio Meta-chips, University of Electronic Science and Technology, Chengdu 611731, P.R. China

* Corresponding author. Email: lurw@dlut.edu.cn; chzouwei@suse.edu.cn

† These authors contributed equally to this work.

Table of Contents

1. Materials and Instrumentation

1.1 Materials

The procurement of all compounds and solvents was meticulously conducted from renowned suppliers, ensuring the highest purity and quality standards. Specifically, NMR solvents including Chloroform-D, deuterated acetonitrile, and Dimethyl Sulfoxide-D6 of anhydrous grade were sourced from Adamas-beta® Reagent Co., Ltd. Moreover, a diverse array of solvents utilized in experimental procedures were acquired from esteemed suppliers such as Aladdin's Reagent Co., Adamas-beta® Reagent Co., Ltd., and *J&K* Scientific Reagent Co., Ltd. In the subsequent phase, analytical-grade reagents encompassing a broad spectrum of chemicals (dichloromethane, acetonitrile, *N*, *N*-dimethylformamide, toluene, xylene, ethyl acetate, hexane, methanol, ethanol, dimethyl sulphoxide, isopropanol) underwent meticulous dehydration and distillation processes. These procedures were conducted adhering to standardized purification methods, executed in an inert argon atmosphere to ensure the absence of moisture and other contaminants. Further, the incorporation of 5 Å molecular sieves facilitated the maintenance of an anhydrous state in which the materials were securely stored. Additionally, high-purity electronic grade reagents including Bismuth (III) fluoride (BiF_3), Copper (II) fluoride (CuF_2), and Cerium (Ce) were obtained from Sente Target Co. The chemical inventory was further enriched with the acquisition of Neopentylamine (98%), pivalaldehyde (96%), paraformaldehyde (95%), formic acid (HCOOH; 99%), magnesium sulfate ($MgSO_4$; 99.5%), iodomethane (CH_3I; 99%), potassium carbonate (K_2CO_3; 99.5%), Indium (III) bromide ($InBr_3$; 99.95%), triethylsilane (Et_3SiH; 98%), silver fluoride (AgF; 99.9%), trifluoroacetic acid (TFA; 99%), and triethylamine (99%) from Aladdin's Reagent Co. Furthermore, carbon nanotubes, pivotal to several experimental protocols, were procured from Chengdu Organic Chemistry Co. Lastly, the bonding agent utilized, polyvinylidene fluoride (PVDF), of electronic grade, was sourced from Arkema, thereby ensuring the adherence to stringent quality benchmarks essential for the success of the experimental endeavors.

1.2 Instrumentation

Scanning electron microscopy (SEM) analyses were conducted using a Thermo Scientific Apreo 2C instrument. The negative electrode material was mounted onto a conductive adhesive within an argon atmosphere, followed by the deposition of an approximately 2 nm thick gold layer to enhance conductivity. The sample was maintained in an inert environment from fabrication through testing to preserve its integrity. Transmission electron microscopy (TEM) imaging was performed using a Talos F200S microscope at an accelerating voltage of 200 kV. Analytical characterizations were augmented using SUPERX energy-dispersive X-ray spectroscopy (EDS). To obtain representative samples, the negative electrode material was sectioned with a Thermo Scientific Helios 5 CX focused ion beam (FIB). Film materials were analyzed using a Rigaku Smartlab 9 kW grazing incidence X-ray diffractometer (GIXRD) at a 1-degree incident angle. The crystal structure and phase purity of synthesized materials were examined using X-ray diffraction (XRD) with Cu Kα1 radiation on a Nihon Rigaku Ultima IV instrument. All analyses were conducted under non-destructive testing conditions with continuous inert gas protection from sample preparation to testing. X-ray photoelectron spectroscopy (XPS) analyses were carried out using a Thermo Scientific K-Alpha+ high-resolution spectrometer with Al Kα X-rays as the excitation source. Sample preparation for XPS was done in a glove box under inert or vacuum conditions to prevent contamination and solvent interference. Precautions included depressurizing the circulating electrode materials to remove surface solvents, followed by storage in an inert atmosphere. XPS data were calibrated against the carbon 1s peak (284.8 eV), with peak deconvolution and fitting performed using Avantage software. Organic product analysis was conducted using ^{1}H-NMR, ^{13}C-NMR, and ^{19}F-NMR spectroscopy on a Bruker 400 MHz NMR instrument.

Extended X-ray absorption fine structure (EXAFS) measurements were conducted at the 5S1 X-ray absorption beamline of the Aichi Synchrotron Radiation Center. This beamline features a double-bounce channel-cut Si (111) monochromator. The end-station is equipped with advanced detectors for both transmission and fluorescence mode spectroscopy, accommodating a wide range of photon fluxes

across various energy modes. Soft X-ray absorption spectroscopy measurements were performed on the sample at beamline 20A1 of the Taiwan Light Source (TLS) at the National Synchrotron Radiation Research Center (NSRRC). The HSGM beamline, an early version of the Dragon beamline, uses spherical optical elements and a movable exit slit to maximize photon throughput and energy-resolving power. It consists of one horizontal focusing mirror (HFM), one vertical focusing mirror (VFM), one spherical grating monochromator with four gratings, and one toroidal refocusing mirror. This beamline covers the spectral range from 60 eV to 1250 eV, with an average energy resolving power of 5000. Data pretreatment and EXAFS fitting were performed using the Ifeffit software package.[1]

2. Synthetic Procedures

2.1 Synthesis of Dimethyldineopentylammonium fluoride

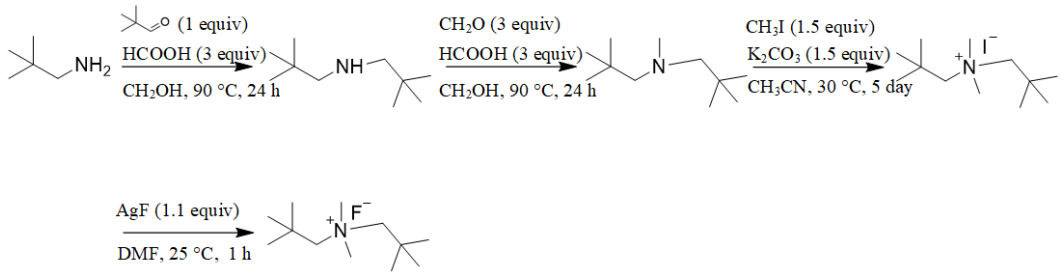

Figure S1. Synthesis process for *β*-H-free fluoride ion quaternary ammonium salts

Dineopentylamine: In this experiment, a three-necked flask was employed for the synthesis of dineopentylamine. Neopentylamine (11.7 mL, 100 mmol) was initially introduced into the flask, followed by the sequential addition of anhydrous magnesium sulfate (14 g, 100 mmol), neopentylaldehyde (12.1 mL, 110 mmol), and 100 mL of methanol. Formic acid (11.32 mL, 300 mmol) was then added dropwise to the reaction mixture. The reaction temperature was subsequently elevated to 80 °C, and the mixture was maintained at this temperature for 20 hours. After this period, the reaction system was allowed to cool to room temperature. A 1 M NaOH solution was gradually added until the pH of the system reached approximately 8. The aqueous layer was extracted three times with 100 mL of ethyl acetate each time. The organic

phase (upper layer) was separated, dried over anhydrous magnesium sulfate, and concentrated under reduced pressure. The final product was purified by recrystallization using a 1:1 mixture of ethyl acetate and hexane. White solid, yield 95%. m.p. 46 °C; ^{1}H-NMR (400 MHz, Chlorform-d) δ: 2.82 (s, 4H), 1.09 (s, 18H); ^{13}C-NMR (400 MHz, Chloroform-d) δ: 61.25, 31.18, 27.54.

***N*,2,2-trimethyl-*N*-neopentylpropan-1-amine:** Dineopentylamine (5.58 g, 36 mmol) was initially added to the reaction flask, followed by the addition of a 37% aqueous formaldehyde solution (17.5 mL, 216 mmol) and formic acid (5 mL, 216 mmol). After these reagents were combined, 100 mL of methanol was introduced. The temperature of the mixture was then increased to 80 °C. Thin-layer chromatography (TLC) was employed to monitor the progress of the reaction, using alkaline potassium permanganate as the color developer. The reaction was deemed complete when the starting material was no longer detectable. To neutralize the excess formic acid, a 1 M NaOH aqueous solution was added gradually. Following neutralization, the solvent was removed via evaporation under reduced pressure. The residue was then diluted with 100 mL of deionized water and extracted with 100 mL of ethyl acetate, repeating the extraction process three times. The resulting organic phase was isolated, dried over anhydrous magnesium sulfate, and concentrated by evaporation to obtain the crude product. This crude product was further purified via flash column chromatography. Colorless clear liquid, yield 70%. b.p. 180 °C; ^{1}H-NMR (400 MHz, Chlorform-d) δ: 2.32 (s, 3H), 2.21 (s, 4H), 0.90 (s, 18H); ^{13}C-NMR (400 MHz, Chloroform-d) δ: 74.56, 48.13, 33.39, 28.81.

Dimethyldineopentylammonium iodine: A 100 mL three-necked flask was utilized for the synthesis. Initially, *N*,2,2-trimethyl-*N*-neopentylpropan-1-amine (2.34 mL, 20 mmol) and iodomethane (1.87 mL, 30 mmol) were introduced into the flask, followed by the addition of 50 mL of dimethylformamide (DMF). The reaction was conducted at room temperature, shielded from light, over a period of 5 days. After this duration, the solvents were removed by distillation under reduced pressure, yielding a white

crude product. This product was then recrystallized using a 5:1 mixture of ethyl acetate and methanol. Following recrystallization, the product was filtered and washed with ethyl acetate. The final drying process was carried out in a vacuum oven at 40 °C for 12 hours, resulting in the purified product.

Dimethyldineopentylammonium fluoride: Within a glove box, a purified and de-watered acetonitrile solution (20 mL) was added to a 50 mL polytetrafluoroethylene (PTFE) reaction flask. This was followed by the introduction of a solution containing silver fluoride (AgF, 1.40 g, 11 mmol) and an iodide salt (3.13 g, 10 mmol). The mixture was stirred at room temperature for 2 hours. After this period, solid materials were separated using a needle filter. The filtered mixture was transferred to an electrolytic bath, where it underwent decomposition at 3V for 5 days. This process aimed at the near-complete removal of silver ions and residual water from the system. Subsequently, the solvent was removed by distillation under reduced pressure, with the process carried out under inert gas protection. The resultant product was maintained in the glove box for storage. White solid, yield 45%. ^{1}H-NMR (400 MHz, Chlorform-d) δ: 3.19 (s, 4H), 3.08 (s, 6H), 1.1 (s, 18H); ^{19}F-NMR (400 MHz, Acetonitrile) δ: 74.82 (s, 1F).

2.2 1,1,1-trifluoro-2-(2,2,2-trifluoroethoxy)ethane

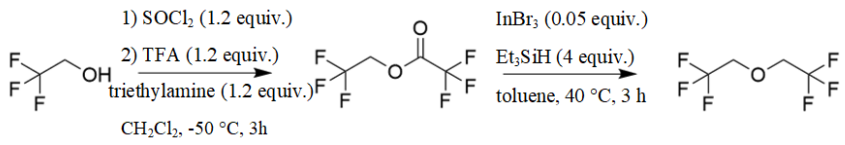

Figure S2. Synthesis scheme of 1,1,1-trifluoro-2-(2,2,2-trifluoroethoxy)ethane

2,2,2-trifluoroethyl trifluoroacetate: The reaction flask was initially subjected to high-temperature drying before the introduction of trifluoroacetic acid (37.1 mL, 500 mmol) under a nitrogen atmosphere. This was followed by the sequential addition of dichlorosulfoxide (43.58 mL, 600 mmol) and 300 mL of dichloromethane. The reaction was allowed to proceed at room temperature for 3 hours, after which the

system was cooled to -50 °C. Trifluoroethanol (35.96 mL, 500 mmol) was then added to the mixture, which was stirred for an additional 30 minutes. Subsequently, triethylamine (83.40 mL, 600 mmol) was added dropwise. After a stirring period of 5 hours, the reaction mixture was poured into 300 mL of ice water. This mixture underwent extraction with dichloromethane, and the resulting organic phase was collected and dried over anhydrous magnesium sulfate. The fraction at 55 °C was isolated through distillation. Finally, the product was further purified using a distillation column. Colorless clear liquid, yield 70%. b.p. 55 °C; ^{1}H-NMR (400 MHz, Chlorform-d) δ: 4.72, 4.70, 4.69, 4.68 (q, *J* = 4 Hz, 2H); ^{13}C-NMR (400 MHz, Chloroform-d) δ: 156.63,156.33, 156.03, 155.74, 77.08, 76.86, 76.05, 62.81, 62.56, 62.30, 62.05. ^{19}F-NMR (400 MHz, Chloroform-d) δ: 77.91, 74.75, 75.85, 77.32.

1,1,1-trifluoro-2-(2,2,2-trifluoroethoxy) ethane: A 150 mL three-necked flask was initially used for this procedure. First, 2,2,2-trifluoromethyl trifluoroacetate (6.7 mL, 50 mmol) and 50 mL of toluene were sequentially introduced into the flask. Then, indium(III) bromide ($InBr_3$, 0.86 g) was added. The system was purged with nitrogen for 10 minutes to create an inert atmosphere. The reaction temperature was then increased to 40 °C. Once a stable temperature was established, triethylsilane (Et_3SiH, 16 mL, 100 mmol) was gradually added dropwise. The reaction was allowed to proceed for 3 hours after this addition. Upon completion of the reaction, the fraction boiling at 60 °C was collected using a distillation apparatus. Finally, the product underwent further purification through a secondary distillation column. Colorless clear liquid, yield 35%. b.p. 60 °C; ^{1}H-NMR (400 MHz, Chlorform-d) δ: 4.01, 4.00, 3.98, 3.97 (q, *J* = 4 Hz, 4H); ^{13}C-NMR (400 MHz, Chloroform-d) δ: 77.15, 76.94, 76.73, 69.66, 69.43, 69.19, 68.96. ^{19}F-NMR (400 MHz, Chloroform-d) δ: 75.92.

2.3 Bismuth trifluoride and lithium fluoride target preparation

A total of 1 kg of either bismuth trifluoride (BiF_3) or lithium fluoride (LiF) was subjected to grinding and mixing using an airflow mill for 3 hours, resulting in a homogeneous powder. The powder was then loaded into a mold and hot-pressed at

180 °C under a pressure of 30 tonnes. Following this initial forming step, the target was transferred to a furnace filled with inert argon (Ar) gas. The temperature in the furnace was gradually increased to 300 °C at a rate of 5 °C per minute and maintained at this level for 30 minutes. Subsequently, the temperature was further elevated to 680 °C at a rate of 10 °C per minute and sustained at this peak for 3 hours. After the high-temperature treatment, the temperature was decreased to room temperature at a rate of 5 °C per minute. Once the target had cooled down, it was affixed to a high-purity copper mold. The final step involved polishing the target to achieve the required specifications for the bismuth fluoride oxide target needed for this study.

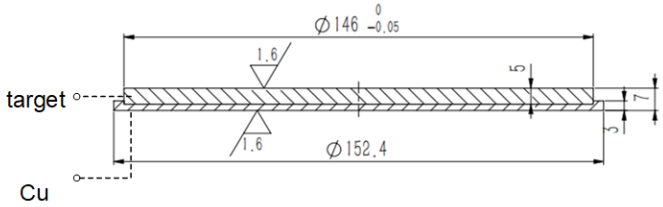

Figure S3. Schematic of BiF_3 and LiF targets used in RF sputtering

2.4 Electrode sheet preparation

Electronic grade polyvinylidene fluoride (PVDF) was used as a binder for both the positive and negative electrodes. The binder was mixed with the active substance and hydroxyl-free carbon nanotubes in a weight ratio of 1.8:0.5:0.5 (active substance: carbon nanotubes: PVDF). This mixture was uniformly ground in a mortar and pestle, then stirred in an inert atmosphere using anhydrous DMF as the solvent. The resulting paste was cast onto the current collector using a spatula within a glove box. The material was subsequently dried under vacuum at 100 °C for 12 hours. After drying, the material was fashioned into 14 mm diameter discs using a press blade. The anode's active material comprised cerium (Ce) powder, and all experimental procedures and transportation were conducted under strictly anhydrous and oxygen-free conditions. To ensure the removal of adsorbed water, all glassware and model CR2025 coin cell materials were pre-dried in a vacuum oven at 100 °C for 8 hours. This was followed by replacement with argon gas and transfer to a glove box through an airbag, maintaining an inert gas atmosphere. Within the glove box, the levels of O_2 and H_2O were meticulously controlled to remain below 0.1 ppm.

2.5 Accumulation of buffer phases on negative electrode sheets by RF sputtering

The device's schematic, depicted in **Figure S5**, comprises three principal components: (1) source ion implantation, (2) RF-sputtering source, and (3) plasma device. The electrode sheet was affixed onto a 10×10 cm, 5 mm-thick stainless steel plate using conductive adhesive within an argon environment. This assembly was then transferred into the device under an inert gas atmosphere. The system was evacuated to achieve a pressure of 1 mTorr, followed by argon infusion to stabilize the pressure at 9 mTorr. Initially, the electrode sheet underwent plasma activation for 10 minutes. After this period, the activated electrode sheet was precisely aligned opposite the RF sputtering source. A robotic arm controlled the sputtering energy and duration, which were crucial for adjusting the crystalline phase and thickness of the modified layer. Upon completion of the experiment, the material was transferred to a glove box under an inert gas atmosphere to ensure its preservation.

2.6 Electrochemical measurements

The electrode materials employed in this study were BiOF–CuF_2 (Cathode) and LiF–Ce (Anode), prepared as detailed in the preceding section. These materials were assembled within an argon-filled glove box, characterized by exceedingly low water (H_2O < 0.01 ppm) and oxygen (O_2 < 0.1 ppm) levels. The electrolyte, selected from a range of pre-prepared fluoride salts, was formulated as a 0.75 M fluoride ion electrolyte solution using BTFE solvent synthesized in-house. Prior to usage, the electrolyte's water content was rigorously assessed using the Karl Fischer titration method to ensure the residual water content in the solution did not exceed 1 ppm. If the criterion was not met, further purification of the electrolyte was performed. Subsequent testing of the system was conducted using a CHI760E electrochemical workstation (Chenhua, Shanghai, China) and a Wuhan LAND battery testing system (25 °C).

All three-electrode system cells used titanium mesh as the counter electrode and Ag/AgCl as the reference electrode. Linear scanning voltammetry (LSV) was performed on a CHI760E electrochemical workstation (Chenhua, Shanghai, China) at

a scan rate of 1 mV s^{-1}, with 0.5 mL of electrolyte in the three-electrode system at voltages ranging from –2.0 V to 4.0 V. The working electrode consisted of a PVDF paste coated on stainless steel. CuF_2||Ce, CuF_2||LiF–Ce, and BiOF–CuF_2||LiF–Ce cells were charged and discharged galvanostatically (GCD) using a Wuhan LAND battery testing system at 25 °C. Electrochemical impedance spectroscopy (EIS) analysis was carried out using a Tatsunhua electrochemical workstation, with measurements taken from 100 kHz to 0.01 Hz. The EIS data were used to determine the impedance of CuF_2||Ce, CuF_2||LiF-Ce, and BiOF-CuF_2||LiF-Ce cells, and further used to calculate the ion diffusion coefficient (D) (**Formula 1** and **2**) and activation energy barrier (Ea). To calculate Ea, the charge transfer resistance (R_{ct}) of CuF_2||Ce, CuF_2||LiF-Ce, and BiOF-CuF_2||LiF-Ce cells was measured at different temperatures (from 5 °C to 45 °C) and open-circuit voltages were recorded. The activation energy barrier (Ea) was then obtained using the Arrhenius equation (**Formula 3**). The ionic conductivity of the electrode material at various temperatures was determined using the **Formula 4**.

$$\mathrm{D} = \frac{1}{2}\frac{(RT)^2}{(nAC\sigma F^2)^2} \tag{1}$$

$$Z' = R_s + R_{ct} + \sigma_w \omega^{-0.5} \tag{2}$$

Where R is the universal gas constant, T is the absolute temperature (in kelvin), A is the electrode area, n is the number of transferred electrons, F is the Faraday constant, C is the F^- ion concentration, Q is the Warburg coefficient, and ω is the angular frequency.

$$\frac{1}{R_{ct}} = A \exp\left(\frac{-Ea}{RT}\right) \tag{3}$$

Where R is the universal gas constant, T is the absolute temperature (in kelvin), R_{ct} is the charge transfer resistance.

$$\acute{\mathrm{O}} = \frac{1}{R_{ct}}\frac{L}{S} \tag{4}$$

Where Ó is ionic conductivity, L is thickness of electrode material, and S is Area of electrode material.

Table S1. Ionic conductivity of electrode materials at different temperatures

	CuF_2‖Ce	CuF_2‖LiF−Ce	BiOF−CuF_2‖LiF−Ce
278.15 K	1.11×10^{-5} S cm^{-1}	4.10×10^{-6} S cm^{-1}	6.51×10^{-7} S cm^{-1}
288.15 K	1.99×10^{-5} S cm^{-1}	5.42×10^{-6} S cm^{-1}	1.27×10^{-6} S cm^{-1}
298.15 K	2.19×10^{-5} S cm^{-1}	1.03×10^{-5} S cm^{-1}	1.01×10^{-5} S cm^{-1}
308.15 K	3.25×10^{-5} S cm^{-1}	1.31×10^{-5} S cm^{-1}	1.31×10^{-5} S cm^{-1}
318.15 K	4.65×10^{-5} S cm^{-1}	2.67×10^{-5} S cm^{-1}	2.67×10^{-5} S cm^{-1}

To minimize errors in summarizing the electrode material thickness measurement due to the sampling process, we used an Optosky SM200 (Hunan, China) Optical Thin Film Thickness Measuring Instrument to measure the wet electrode in the field. The volumetric rate of change of the electrode material after operation is calculated using **Equations 5** and **6**.

$$V = \pi r^2 d \tag{5}$$

Where r is Radius of electrode sheets, d is thickness of the electrodes.

$$\text{Volume change} = \frac{V_2 - V_1}{V_1} \times 100\% \tag{6}$$

Table S2. The Rate of volume change of the electrode material after operation

	CuF_2	BiF_3−CuF_2	$BiO_{0.51}F_{1.98}$−CuF_2	$Bi_7O_5F_{11}$−CuF_2	BiOF−CuF_2	Bi_2O_3−CuF_2	BiOF−$CuF_2$500th
d (μm)	66.79	33.22	32.18	31.16	30.19	30.96	32.42
Volume change	202.2%	50.3%	45.6%	41.0%	36.6%	40.1%	46.7%

Note: The initial thickness of the electrode sheet is 22.1 μm, and d represents the thickness of the electrodes.

3. Theoretical calculation

3.1 RF sputtering section

The system energy calculations are performed by using the Vienna ab initio simulation package (VASP) code[2]. The projector augmented wave (PAW) method[3] is used to describe the ionic potential and the Perdew-Burke-Ernzerhof (PBE) functional[4] is used to describe the exchange correlation interactions. The plane-wave kinetic energy cutoff is 500 eV. A 3×3×5 Monkhorst-Pack k-point mesh is used for the Brillouin zone sampling in all the calculations[5]. For structure relaxation, the energy convergence criteria for electronic relaxation is 1×10^{-5} eV, and the ionic relaxation is performed until all forces are smaller than 0.01 eV $Å^{-1}$. The Ab initio molecular

dynamics (AIMD) simulation is employed to similation the temperature changes during reactions. The free energy(ΔG) of each reduction step was obtained at zero bias potential using.[6]

$$\Delta G = \Delta E + \Delta E_{ZPE} + T\Delta S \quad (7)$$

where ΔE was the reaction energy, ΔE_{ZPE} was the difference in zero-point energies, T was the temperature (408K) and ΔS is the reaction entropy.

3.2 Diffusion energy barriers and rate of change of volume

All DFT calculations were performed using the Vienna Ab initio Simulation Package (VASP)[2]. The PAW[3] pseudopotential with the PBE[4] generalized gradient approximation (GGA) exchange correlation function was utilized in the computations. The cutoff energy of the plane waves basis set was 500 eV and a Monkhorst-Pack mesh of 2×2×1 was used in K-sampling. All structures were spin polarized and all atoms were fully relaxed with the energy convergence tolerance of 10^{-5} eV per atom, and the final force on each atom was < 0.05 eV $Å^{-1}$. Finally, the adsorption energies (E_{ads}) were calculated as $E_{ads} = E_{ad/sub} - E_{ad} - E_{sub}$, where $E_{ad/sub}$, E_{ad}, and E_{sub} are the total energies of the optimized adsorbate/substrate system, the adsorbate in the structure, and the clean substrate, respectively. The free energy was calculated using the equation:

The F^- ions Migration barriers searches are performed using the Dimer method in the VTST package. The final force on each atom was < 0.1 eV $Å^{-1}$. The TS search is conducted by using the climbing-image nudged elastic band (CI-NEB) method to generate initial guess geometries, followed by the dimer method to converge to the saddle points.

4. Figure Captions

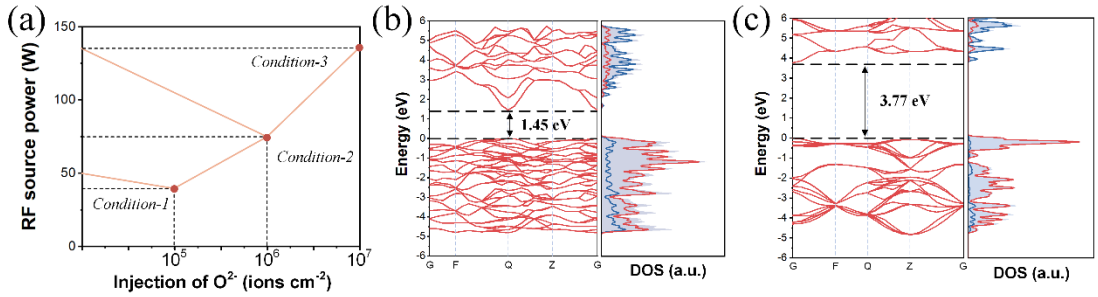

Figure S4 (a) Prediction results of phase diagram by classification for given compositions, and Band Gap and DOS Analysis for (b) Bi_2O_3, (c) BiF_3. [*Condition-1* (40 W, 10^5 ions cm^{-2}), *Condition-2* (75 W, 10^6 ions cm^{-2}), and *Condition-3* (135 W, 10^7 ions cm^{-2})]

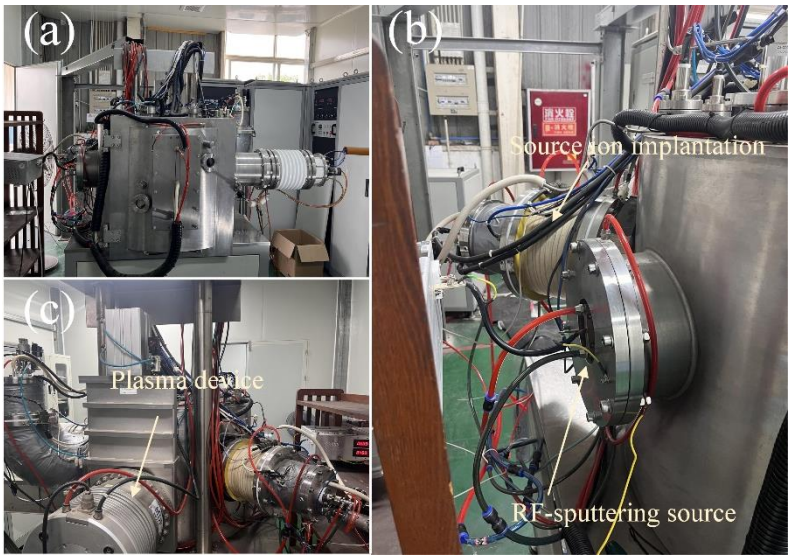

Figure S5. Co-coating Equipment Physical Drawing. (a) General view of the equipment, (b) source ion implantation, RF-sputtering source, and (c) plasma device.

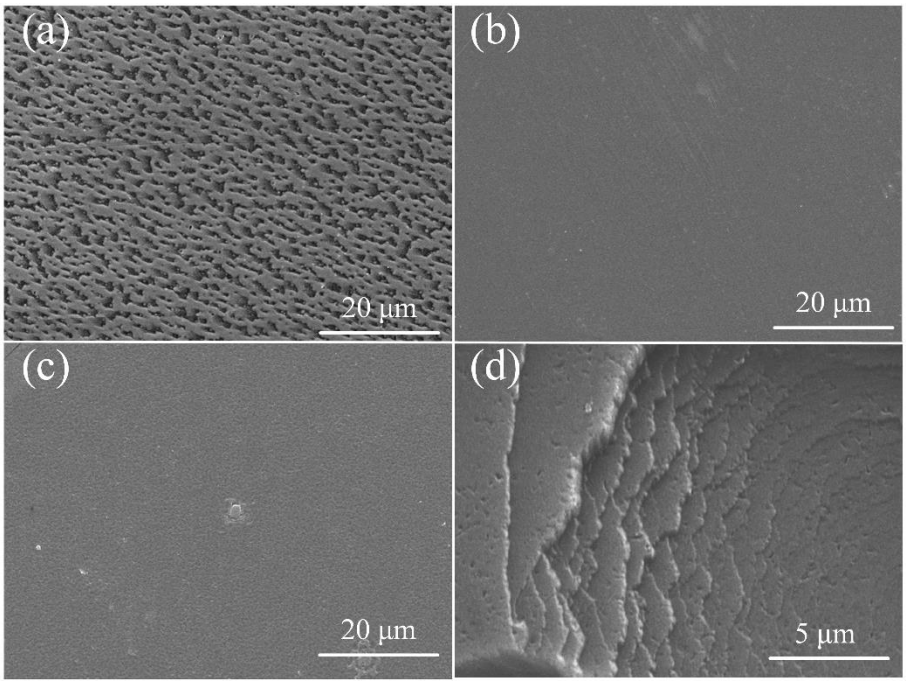

Figure S6. Influence of RF source-substrate distance on film morphology. (a) 30 cm, (b) 15 cm, (c) 10 cm. (d) Topography at the edge of substrate.

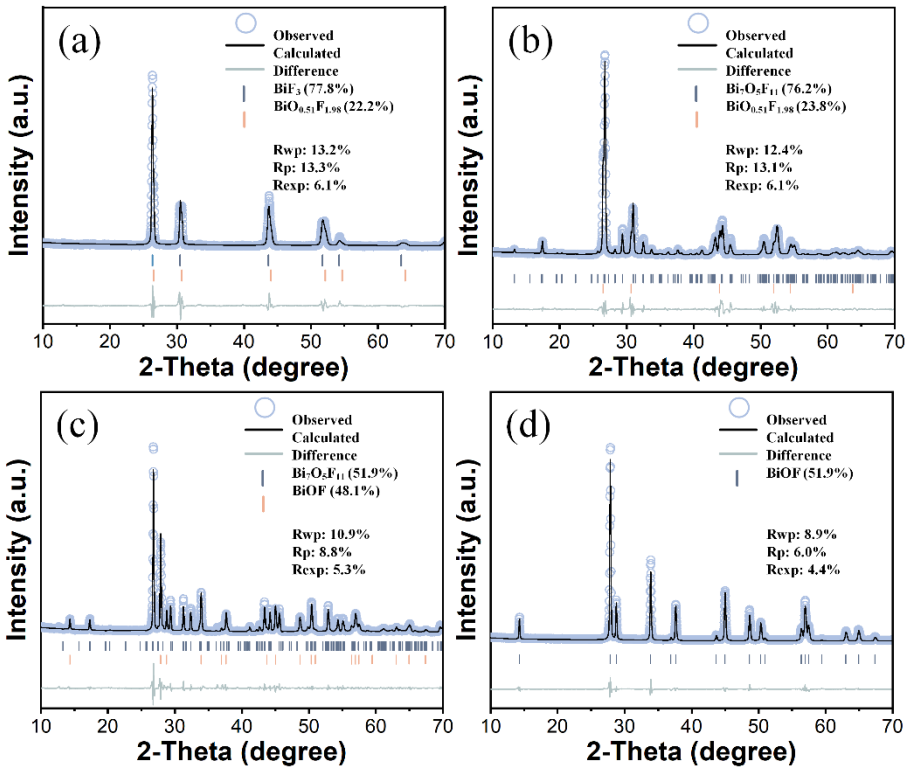

Figure S7. XRD refinements and phase composition analysis. (a) *Condition-1*, (b) *Condition-2*, (c) *Condition-3*, and (d) *Condition-4*.

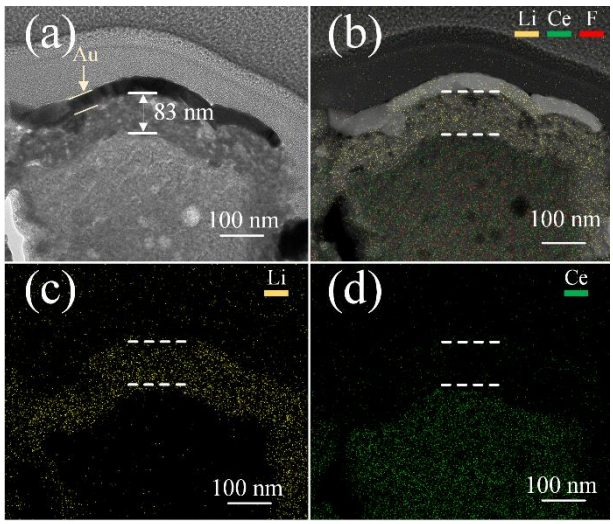

Figure S8. TEM images and corresponding EDS mapping of LiF–CeF_3 anode deposition morphologies.

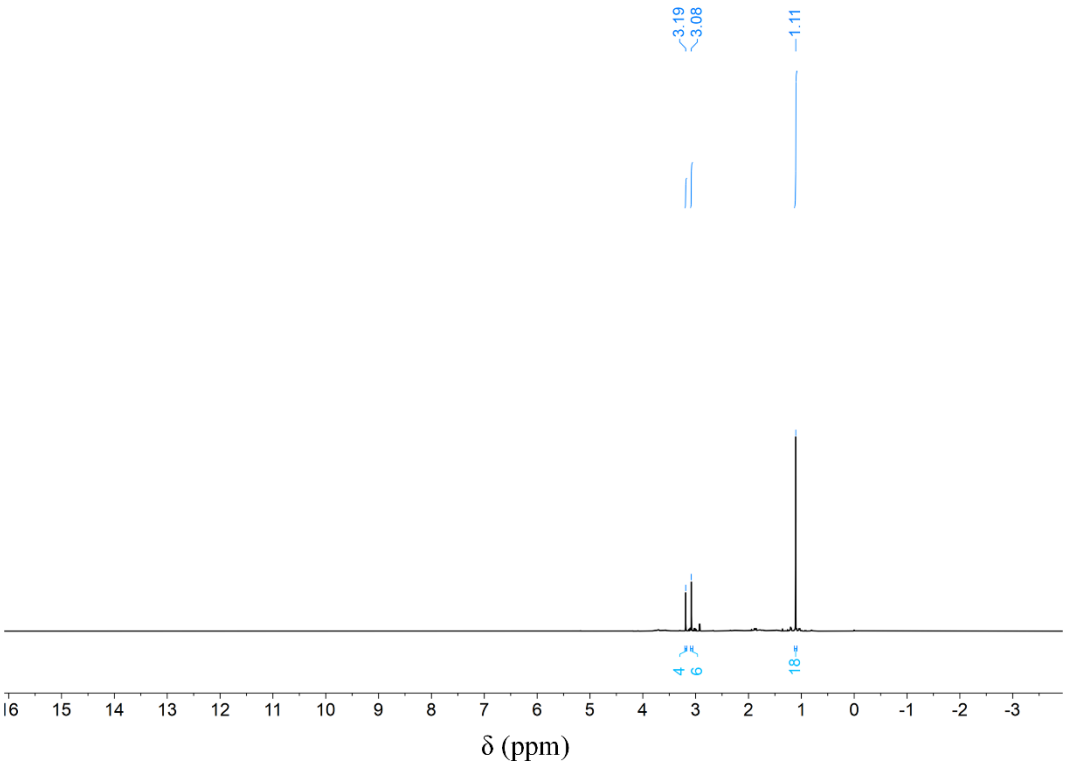

Figure S9. ^{1}H-NMR of dineopentylamine.

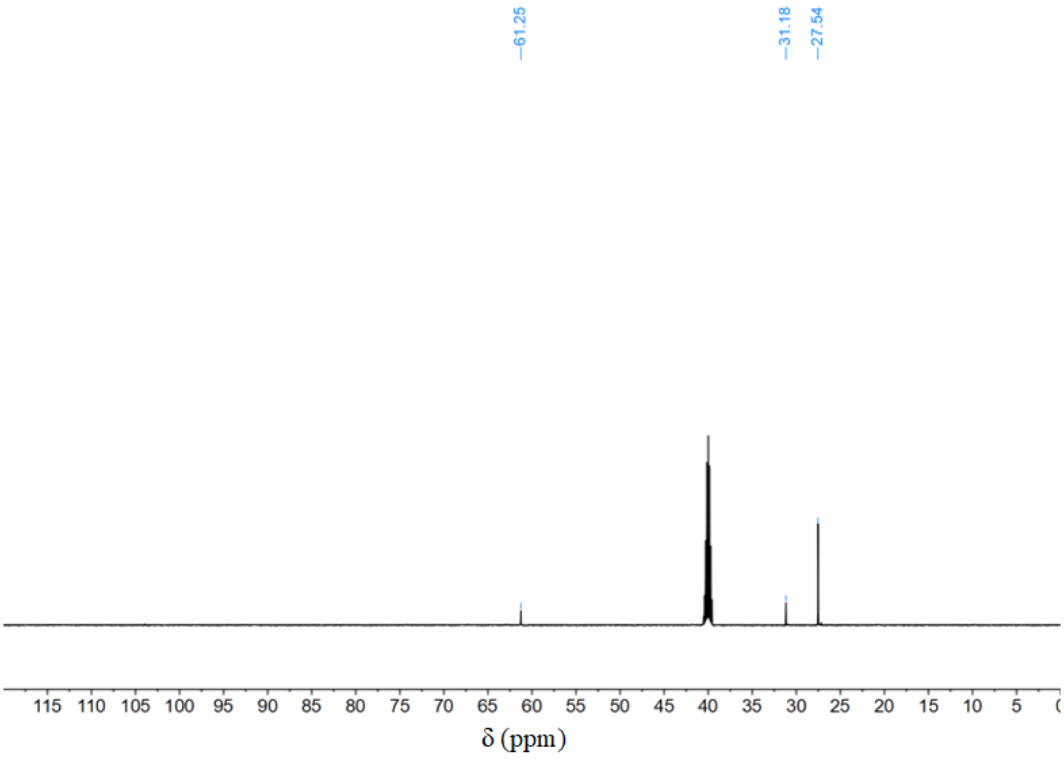

Figure S10. ^{13}C-NMR of dineopentylamine.

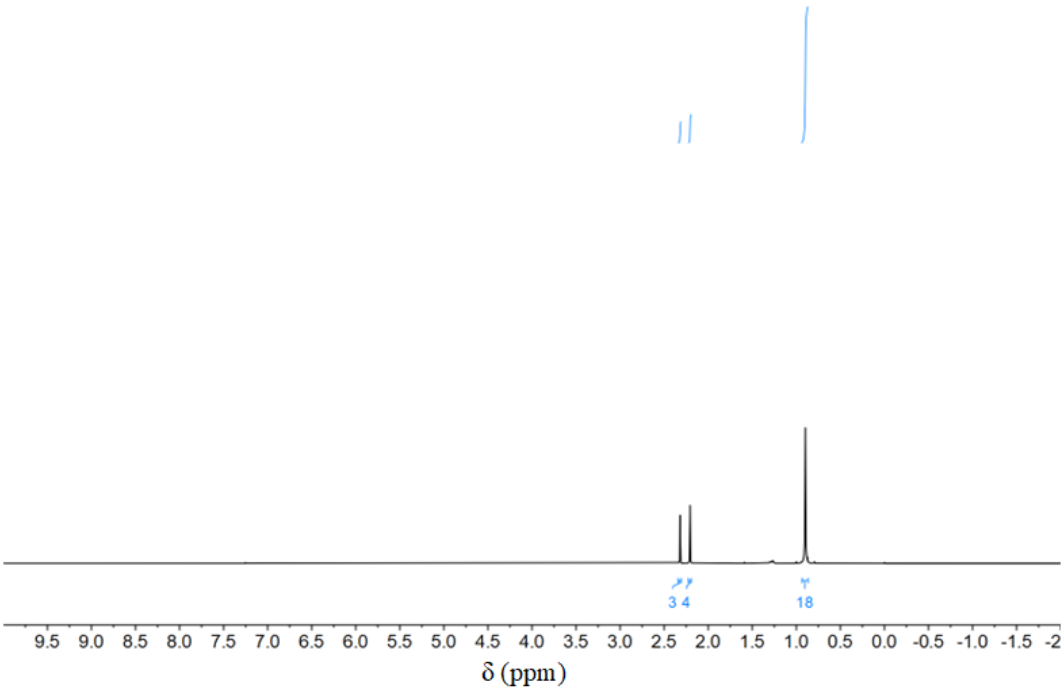

Figure S11. ^{1}H-NMR of *N*,2,2-trimethyl-*N*-neopentylpropan-1-amine

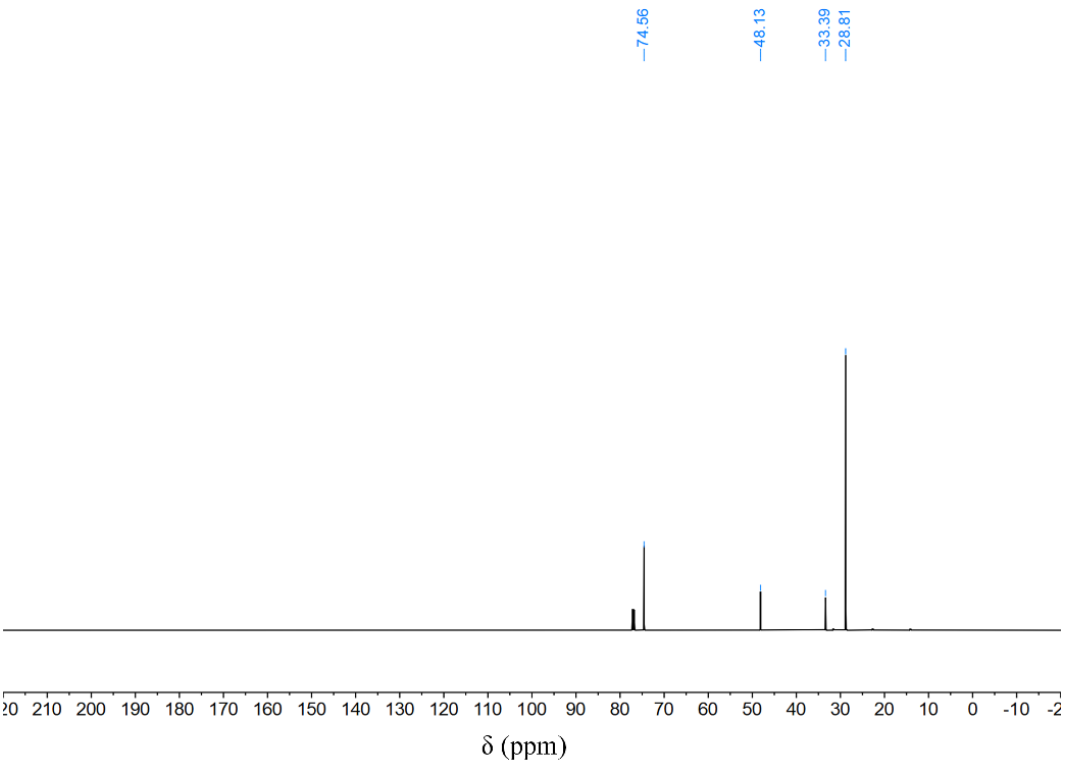

Figure S12. ^{13}C-NMR of *N*,2,2-trimethyl-*N*-neopentylpropan-1-amine.

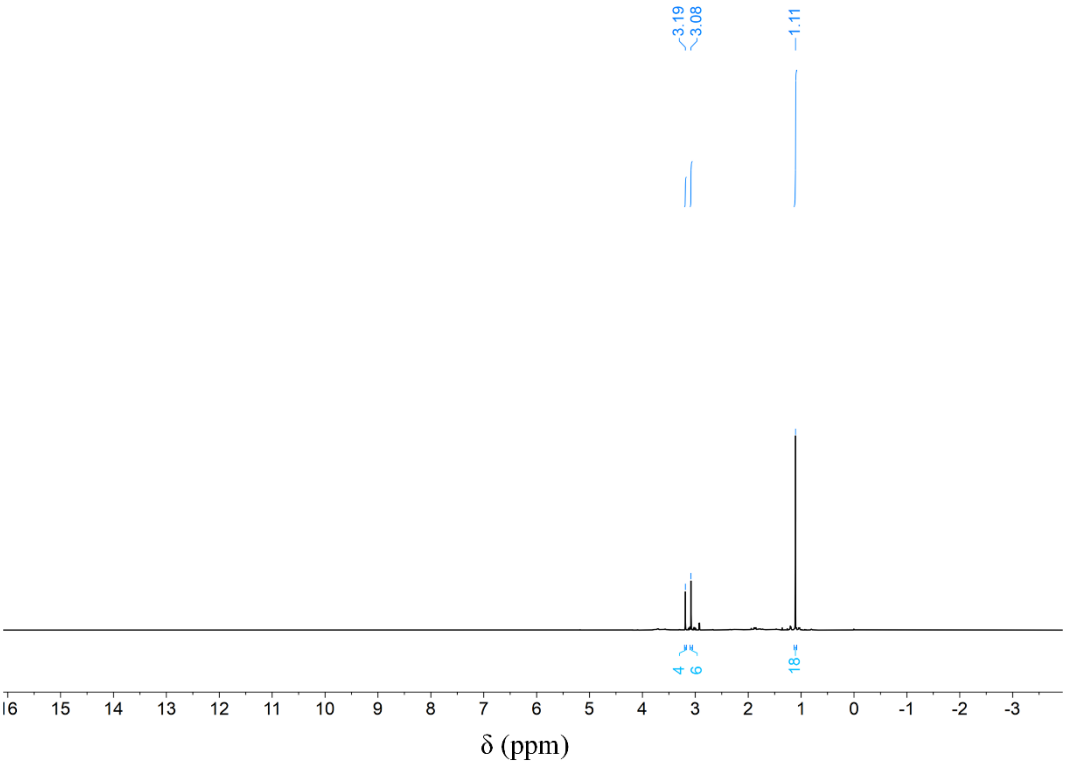

Figure S13. ^{1}H-NMR of dimethyldineopentylammonium fluoride.

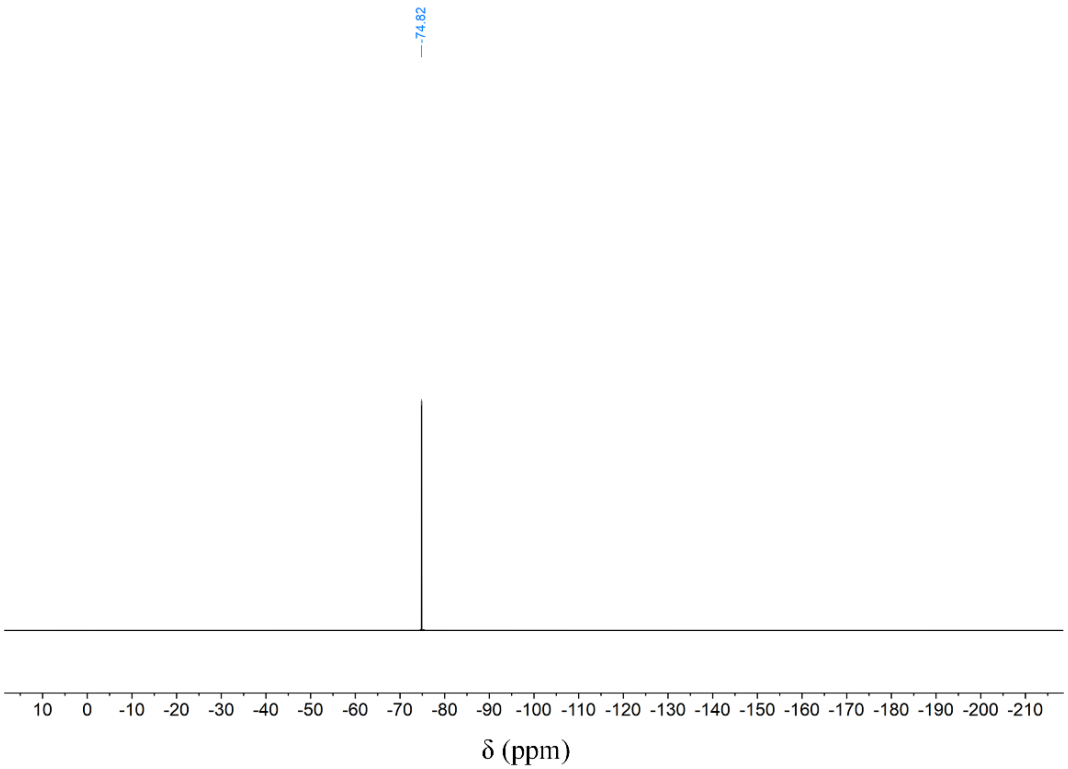

Figure S14. ^{19}F-NMR of dimethyldineopentylammonium fluoride.

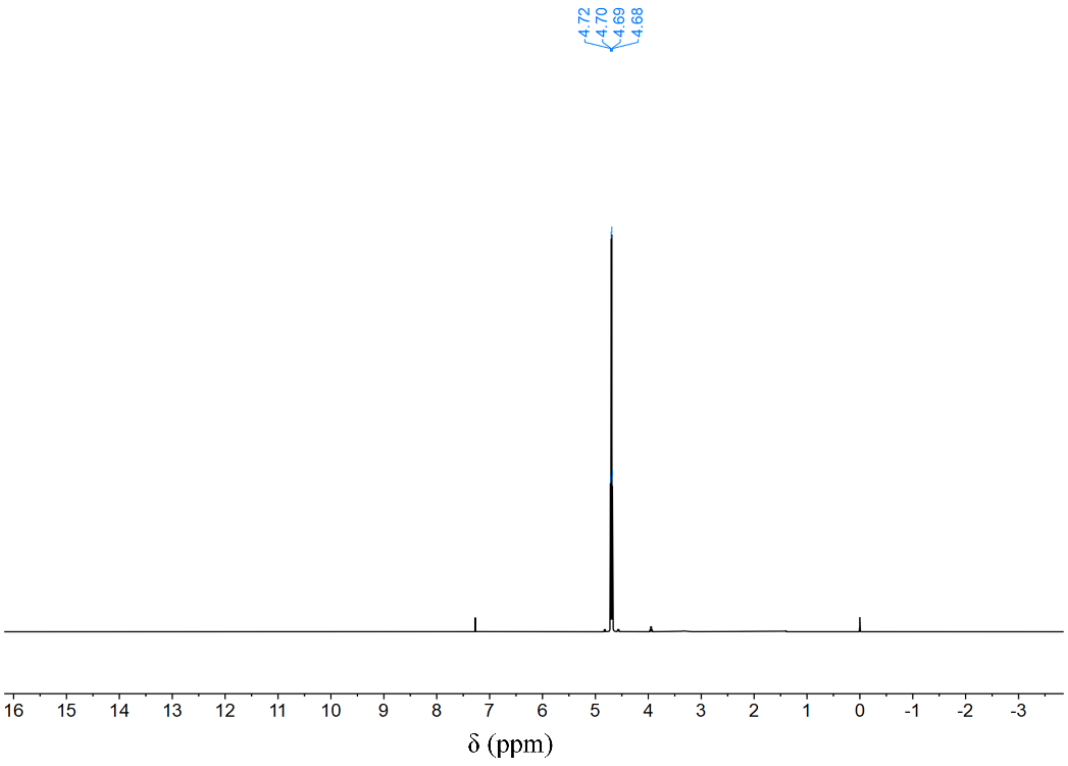

Figure S15. ^{1}H-NMR of 2,2,2-trifluoroethyl 2,2,2-trifluoroacetate.

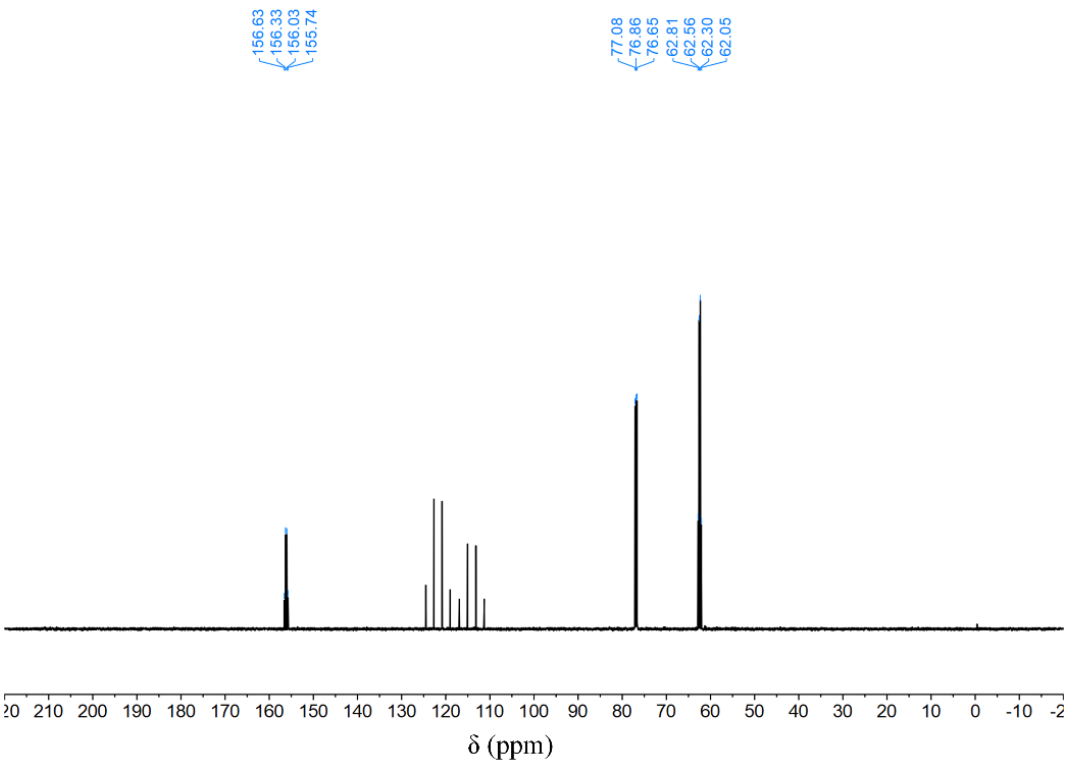

Figure S16. ^{13}C-NMR of 2,2,2-trifluoroethyl 2,2,2-trifluoroacetate.

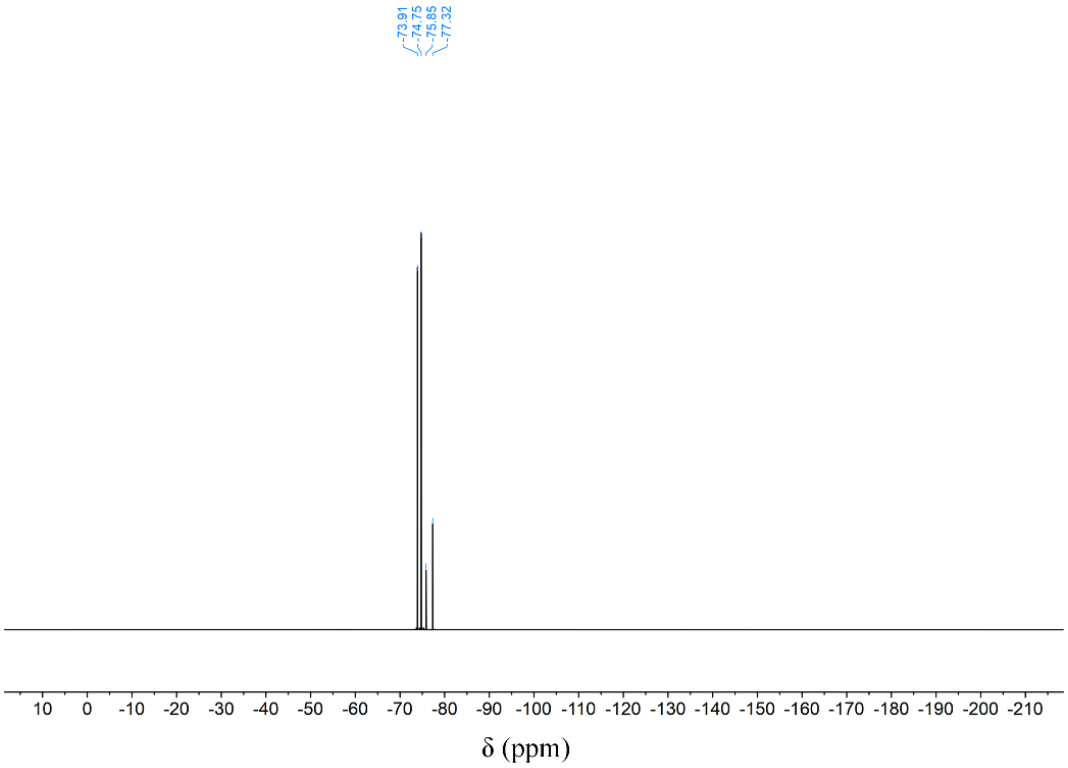

Figure S17. ^{19}F-NMR of 2,2,2-trifluoroethyl 2,2,2-trifluoroacetate.

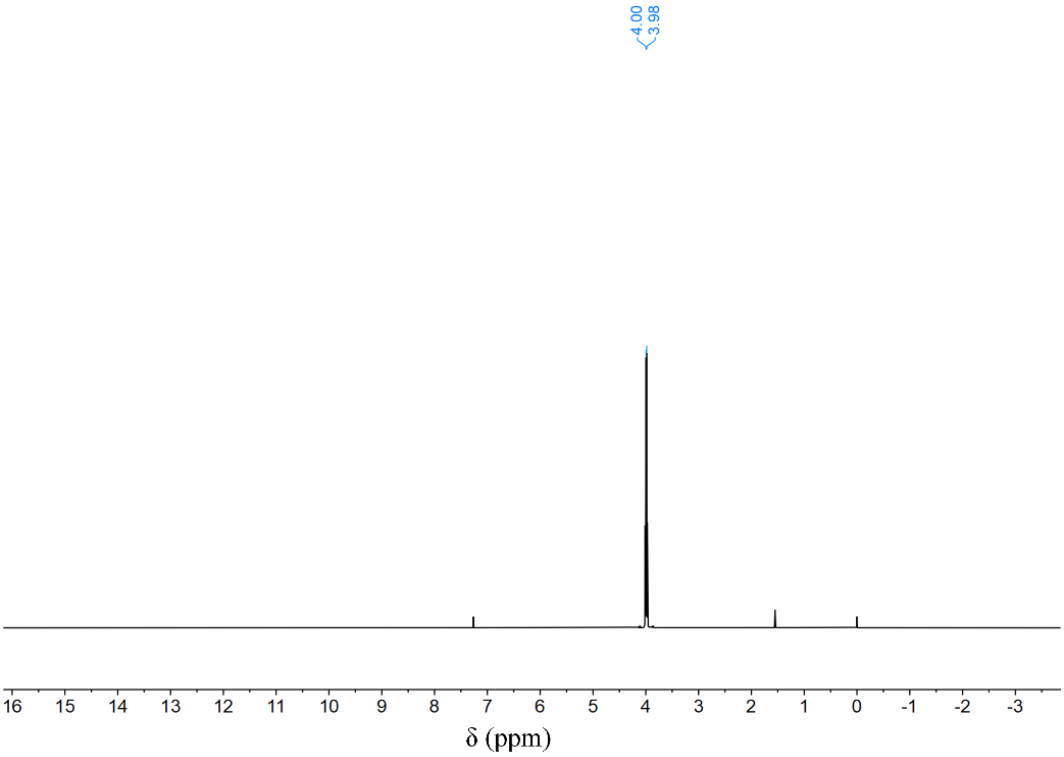

Figure S18. ^{1}H-NMR of 1,1,1-trifluoro-2-(2,2,2-trifluoroethoxy)ethane.

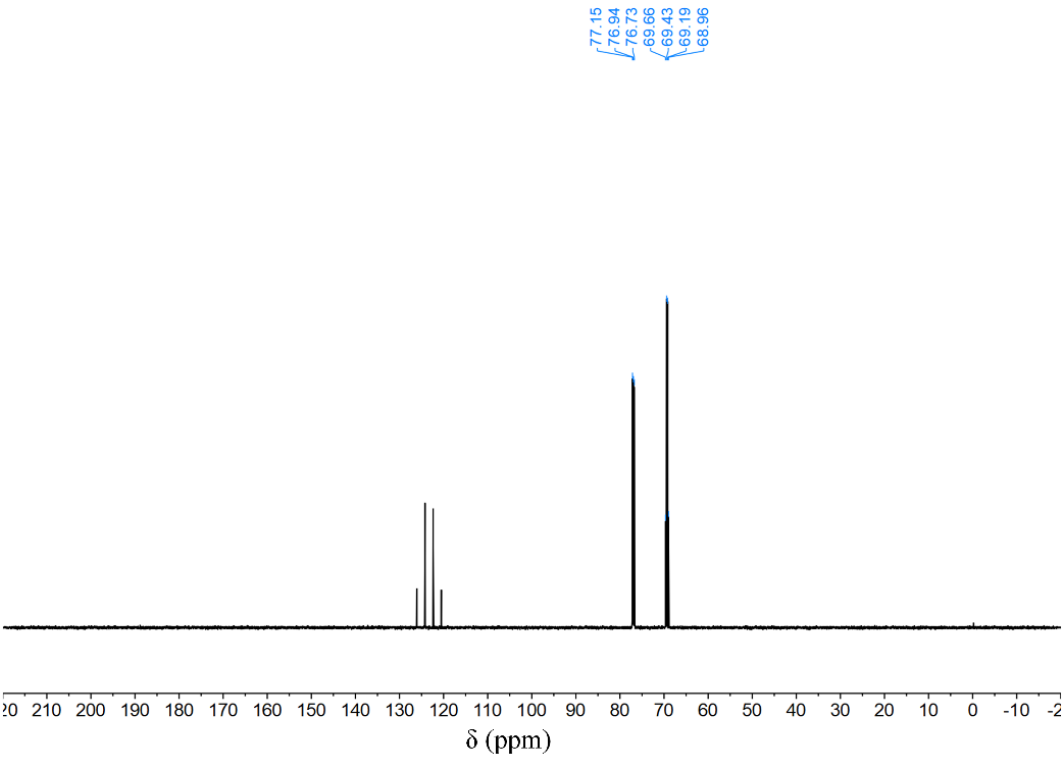

Figure S19. ^{13}C-NMR of 1,1,1-trifluoro-2-(2,2,2-trifluoroethoxy)ethane.

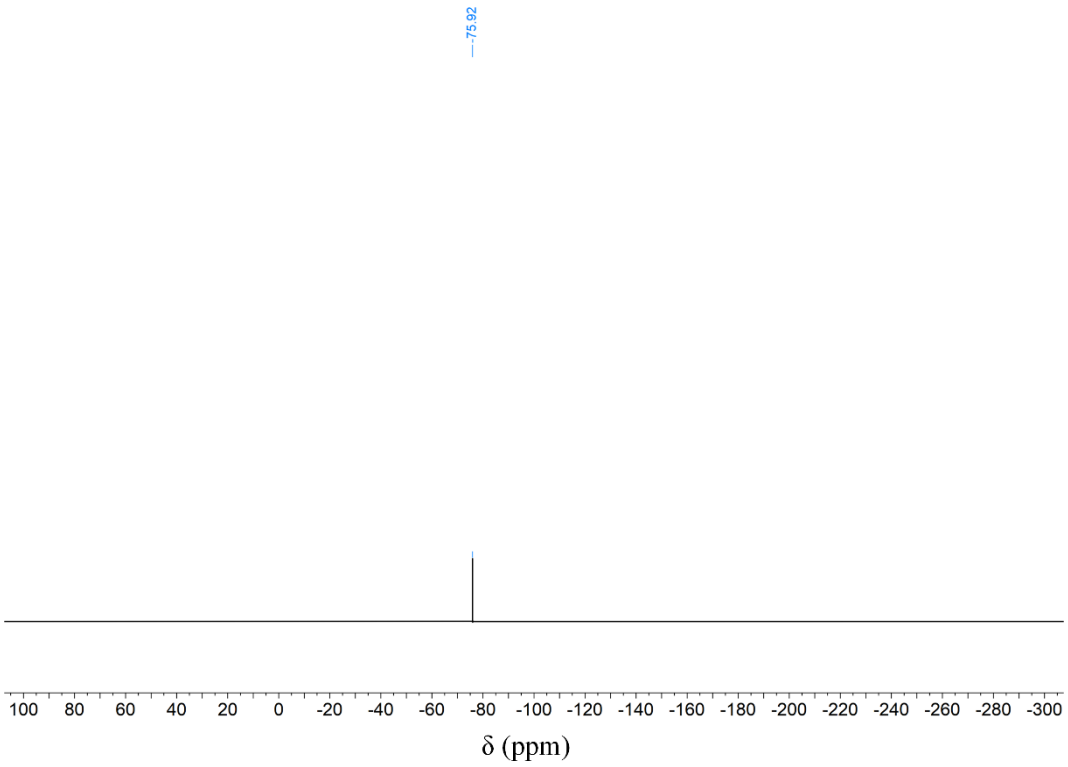

Figure S20. ^{19}F-NMR of 1,1,1-trifluoro-2-(2,2,2-trifluoroethoxy)ethane.

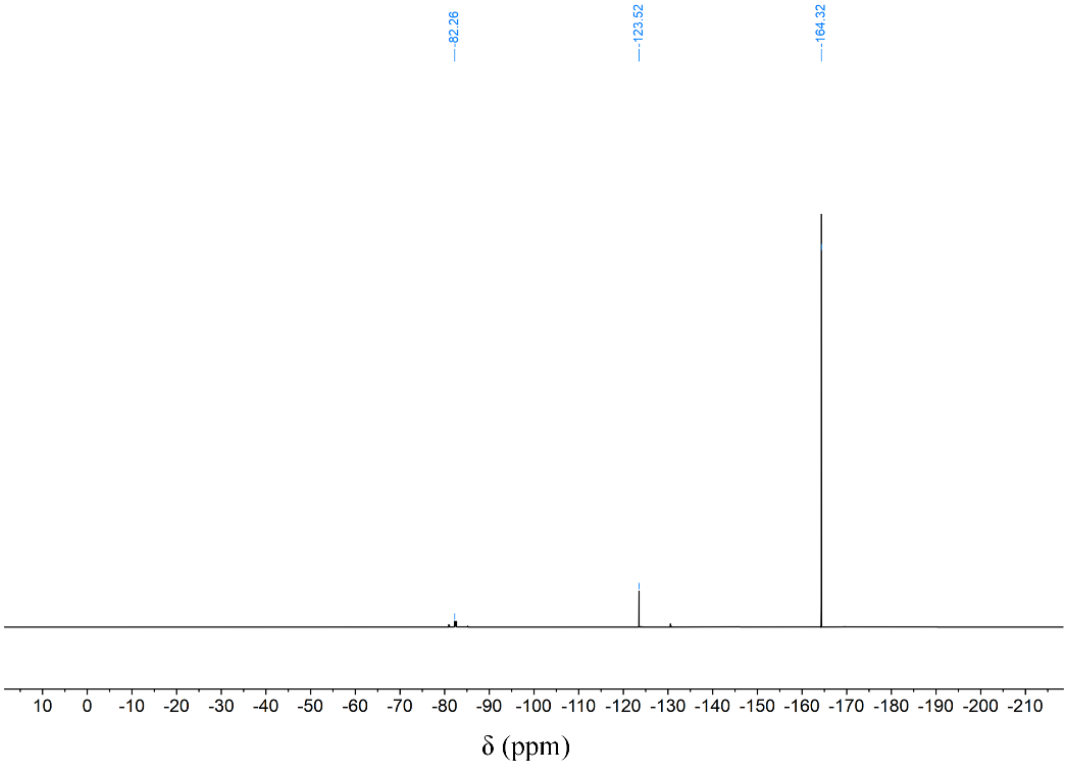

Figure S21. ^{19}F-NMR of the electrolyte using DMF as solvent.

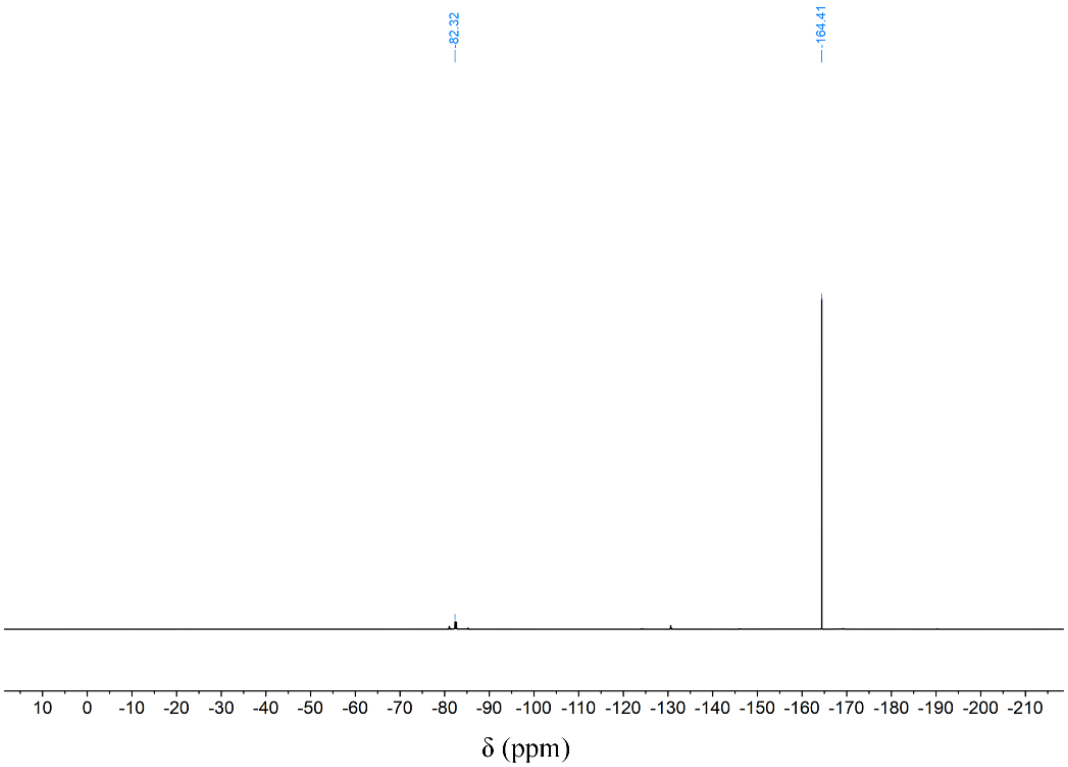

Figure S22. ^{19}F-NMR of the electrolyte using DMSO as solvent.

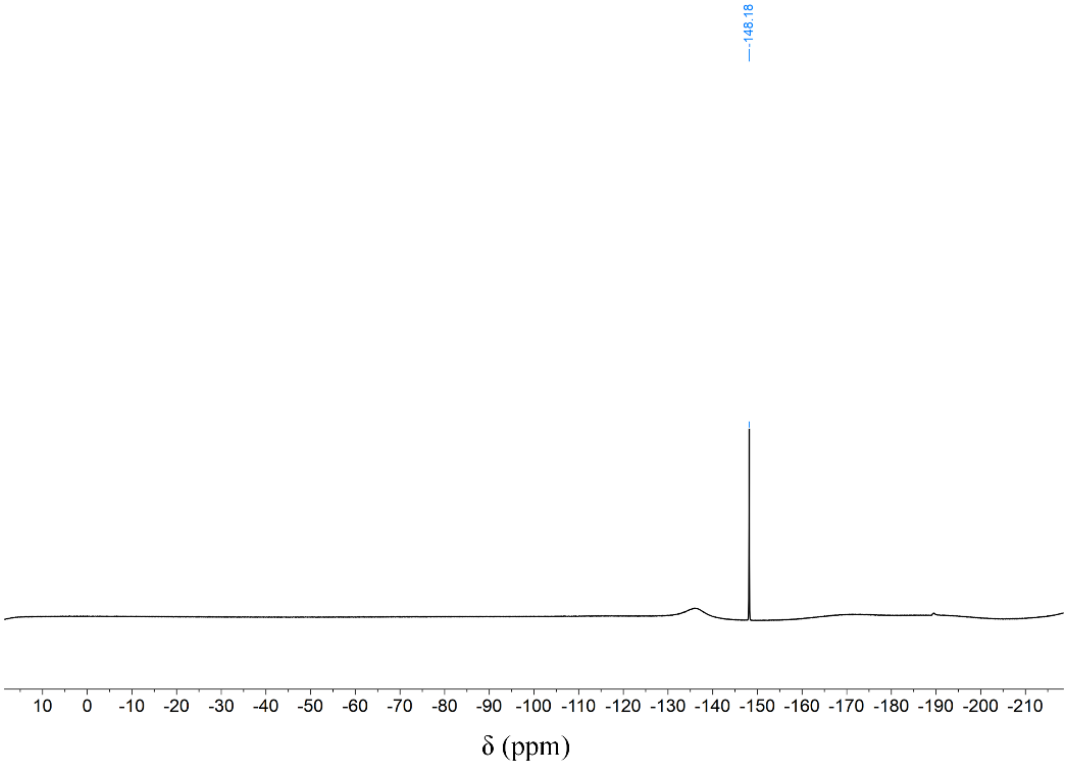

Figure S23. ^{19}F-NMR of quaternary ammonium salts prepared in synthesis using hydrofluoric acid as a fluoride ion exchange source.

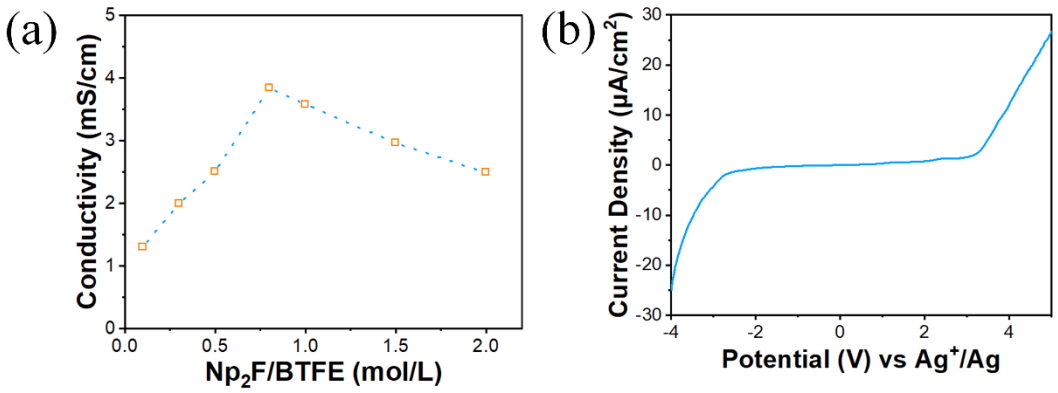

Figure S24. (a) ionic conductivity of Np_2F in liquid BTFE electrolyte solutions as a function of concentration. (b) Linear sweep voltammograms for 0.8 M Np_2F in BTFE.

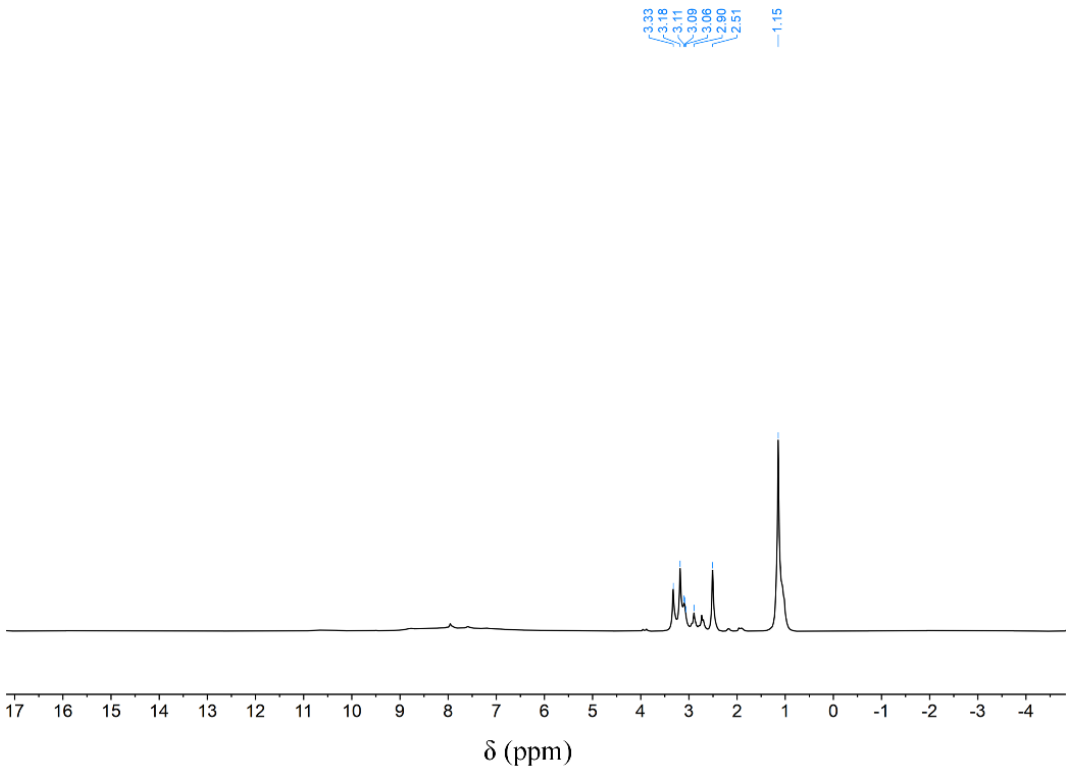

Figure S25. ^{1}H-NMR of the electrolyte after 500 cycles.

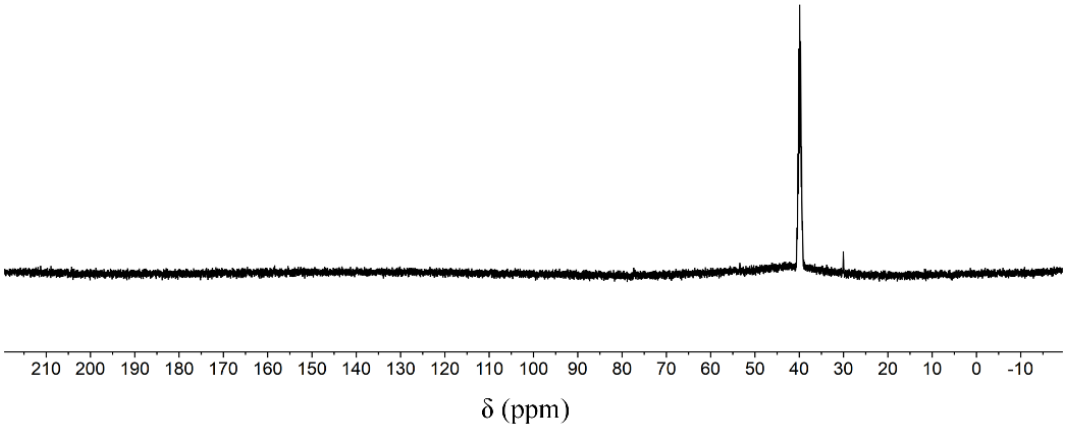

Figure S26. ^{13}C-NMR of the electrolyte after 500 cycles.

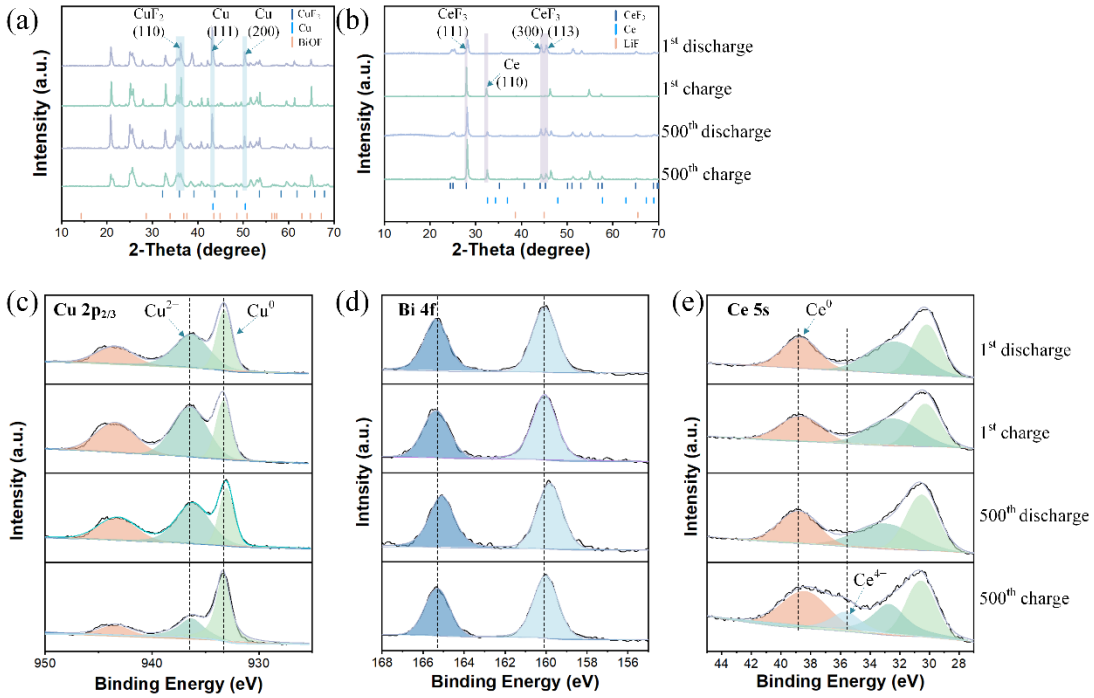

Figure S27. Structures of the cycled electrode materials and characterization to identify the FIEI layer. XRD patterns of (a) BiOF–CuF_2, and (b) LiF–Ce under different charge/discharge states. (c) Cu $2p_{2/3}$, (d) Bi 4f and (e) Ce 5s XPS spectra of electrodes under different charge/discharge states.

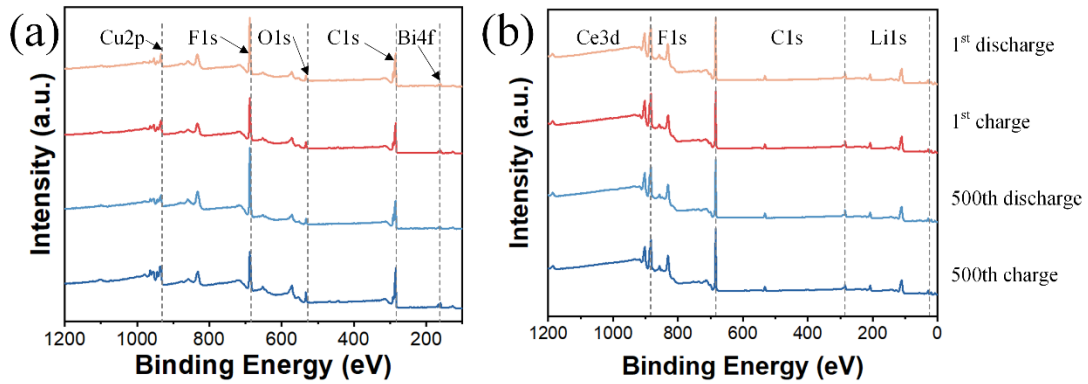

Figure S28. XPS of (a) BiOF–CuF_2 and (f) LiF–Ce under different charge/discharge states.

Table S3. Electrochemical impedance spectra (EIS) of different cells.

	CuF_2‖Ce 1st	CuF_2‖LiF−Ce 1st	BiOF−CuF_2 1st	BiOF−CuF_2 100th	BiOF−CuF_2 500th
R_s	2.9 Ω	3.0 Ω	2.8 Ω	2.6 Ω	2.5 Ω
R_{ct}	35.0 Ω	76.7 Ω	205.5Ω	242.3 Ω	274.7 Ω

Table S4. Structural parameters of different samples extracted from the EXAFS fitting

Shell	CN	R (Å)	σ^2 (10^{-3}Å^2)	ΔE_0 (eV)	R factor
Bi-O	1.3±0.1	2.14±0.01	0.7±0.8	-4.8±1.0	0.014

Data ranges: 3.0 ⩽ k ⩽ 12.0 Å^{-1}, 1.2 ⩽ R ⩽ 3.0 Å. R: bond distance; σ^2: Debye-Waller factors; R factor: goodness of fit. S_0^2 is the amplitude reduction factor (S_0^2 =0.83).

Table S5. Structural parameters of different samples extracted from the EXAFS fitting.

Sample	Shell	CN	R (Å)	σ^2(10^{-3}Å^2)	ΔE_0 (eV)	R factor
BiOF (1st)	Bi-O	1.3±0.1	2.14±0.01	0.7±0.8	4.8±1.0	0.014
	Bi-F	2.1±0.2	2.45±0.01	1.6±0.3		
BiOF (500th)	Bi-O	1.8±0.1	2.15±0.01	3.4±0.8	0.6±1.0	0.012

Bi-F	2.4±0.3	2.47±0.01	2.0±0.3

Data ranges: $3.0 \leq k \leq 12.0$ Å^{-1}, $1.2 \leq R \leq 3.0$ Å. R: bond distance; σ^2: Debye-Waller factors; R factor: goodness of fit. $S0^2$ is the amplitude reduction factor (S_0^2 =0.83);

5. References

[1] Newville, M. IFEFFIT: interactive XAFS analysis and FEFF fitting. *J. Synchrotron Radiat.* **2001**, *8*, 322–324.

[2] G. Kresse, J. Hafner, *Physical Review B*. **2020**, *47*, 558–561.

[3] P.E. Blöchl, *Physical Review B*. **1994**, *50*, 17953–17979.

[4] J.P. Perdew, K. Burke, M. Ernzerhof, *Physical Review Letters*. **1996**, *77*, 3865–3868.

[5] G. Henkelman, H. Jónsson, *The Journal of Chemical Physics*. **2000**, *113*, 9978–9985.

[6] Bartel, C.J., Millican, S.L., Deml, A.M, *Nat Commun*. **2018**, *9*, 4168.